Available online at www.sciencedirect.com
SCIENCE DIRECT®
International Journal of Heat and Mass Transfer 48 (2005) 5058–5071
International Journal of HEAT and MASS TRANSFER
www.elsevier.com/locate/ijhmt

Experiments and modeling of the hydraulic resistance and heat transfer of in-line square pin fin heat sinks with top by-pass flow

M. Baris Dogruoz, Mario Urdaneta, Alfonso Ortega *

Experimental and Computational Heat Transfer Laboratory, Department of Aerospace and Mechanical Engineering, The University of Arizona, Tucson, AZ 85721, USA

Abstract

In pin-fin heat sinks, the flow within the core exhibits separation and hence does not lend itself to simple analytical boundary layer or duct flow analysis of the wall friction. In this paper, we present some findings from an experimental and modeling study aimed at obtaining physical insight into the behavior of square, in-line pin fin heat sinks. In addition to the detailed pressure measurements, the overall thermal resistance was measured as a function of Reynolds number and by-pass height. A "two-branch by-pass model" was developed, in which a one-dimensional difference approach was used to model the fluid flow through the heat sink and its top by-pass duct. Inlet and exit pressure losses were as important as the core pressure drop in establishing the overall flow and pressure drop. Comparisons were made with the data using friction and heat transfer coefficients available in the literature for infinitely long tube bundles of circular cross-section. It was shown that there is a good agreement between the temperature predictions based on the model and the experimental data at high approach velocities for tall heat sinks, however the discrepancy increases as the approach velocity and heat sink height decrease. The validated model was used to identify optimum pin spacing as a function of clearance ratio.

Keywords: Pin fins; Heat sink; In-line arrangement; Hydraulic resistance; Heat transfer; Two-branch by-pass model

1. Introduction

The constant demand for speed and performance in electronics is unfortunately accompanied by ever increasing thermal dissipation. Air heat exchangers or *heat sinks* continue to be the most viable thermal solution for the electronics industry primarily because of low cost and high reliability. Heat sinks for electronics depend on conduction from the electronic package to the heat sink base, followed by conduction into the extended surfaces and convection to the flow. A unique aspect of heat exchangers used in electronics is the possibility that the flow can by-pass the heat exchanger core entirely, and leak from the core to the by-pass duct. Many authors have undertaken the characterization of parallel plate heat exchangers. Knight et al. [1] analytically characterized the flow and heat transfer behavior of such heat exchangers as function of geometry and

* Corresponding author. Tel.: +1 520 621 6787; fax: +1 520 621 8191.
E-mail address: ortega@u.arizona.edu (A. Ortega).

0017-9310/$ - see front matter © 2005 Elsevier Ltd. All rights reserved.
doi:10.1016/j.ijheatmasstransfer.2005.07.004

Nomenclature

A_b	base surface area of a given control volume (m^2)
A_f	area of a single fin exposed to heat transfer (m^2)
A_{fhs}	frontal area of the heat sink (m^2)
A_w	wetted heat sink area (m^2)
a	fin side (m)
BR_{front}	frontal by-pass ratio
BR_o	reference by-pass ratio
b	distance between two fins in the flow direction (m)
CL	clearance ratio (L/H)
c_p	specific heat (J/kg K)
d_f	fin (hydraulic) diameter (m)
H	height of the finned section (fin height) (m)
h	heat transfer coefficient (W/m^2 K)
L	height of the top by-pass section (top clearance) (m)
n	number of rows or columns
P_{st}	static pressure (Pa)
P_{tot}	total pressure (Pa)
P_{L_o}	reference non-dimensional longitudinal pitch
P_L	non-dimensional longitudinal pitch (S_L/d_f)
P_T	non-dimensional transverse pitch (S_T/d_f)
q_{conv}	rate of heat transfer convected through heat sink (W)
q_{loss}	total amount of heat loss (W)
q_{tot}	total power applied to heat sink (W)
R_{th}	base to ambient thermal resistance, Eq. (1), (K/W)
$R_{th,0}$	zero clearance thermal resistance (K/W)
Re_{app}	approach Reynolds number
S_L	longitudinal pitch (m)
S_T	transverse pitch (m)
T	mixed-mean fluid temperature (K)
T_{amb}	ambient temperature (K)
T_b	heat sink base temperature (K)
u	velocity in the finned section (m/s)
u_{app}	approach velocity (m/s)

Greek symbols

δ	uncertainty
ΔP_{core}	core pressure drop in the finned section (Pa)
ΔP_{ent}	pressure drop in the finned section at the entrance (Pa)
ΔP_{ex}	pressure drop in the finned section at the exit (Pa)
ΔP_{tot}	overall pressure drop in the finned section (Pa)
η_o	overall surface efficiency

fluid characteristics, for developing and fully developed flow. Teertstra et al. [2] similarly found analytical solutions for such configurations, and blended both regimes into a single solution for a wide range of Reynolds number. Lee [3] studied the effects of flow by-pass, by allowing flow around the heat exchanger in a partially confined flow configuration. Butterbaugh and Kang [4] treated this case by constructing a nodal network of flow paths, and detailed the calculation of each network element. They accounted not only for flow by-pass, but also for that part of the flow that enters the heat sink and exits through the top, the so-called tip leakage.

In the case of pin fin configurations, however, flow separation and complex three-dimensional flow at the pin-base junction have kept the work on pin fin heat sinks sparse. Simple closed form analytical models of the friction and heat transfer coefficients are not available for either laminar or turbulent regimes. By necessity models thus are simple one-dimensional formulations with empirical formulations of friction and heat transfer coefficients [5,6] or fully conjugate 3-D CFD solutions [7–9].

Except for the pin-end wall effects and tip leakage, the flow within the pin-fin heat sink resembles that within an array of tubes of infinite length. Arrays of circular tubes have been extensively studied [10–12], but detailed experimental data on arrays of tubes of square or rectangular cross-section are rare, except for rectangular cross-sections of large aspect ratio used in in-line and off-set strip fins [7,10,11]. Kays and London [10] present data for infinitely long round tubes in cross flow. Idelchik [11] presents correlations for several different geometries of bundles of tubes. Zhukauskas [12] also presents experimental correlations for tubes in cross flow, as a function of Reynolds number, pin diameter and pitch, with correction factors for longitudinal pitch different to tangential pitch. Data of this type, although not specified for such small heat exchangers as those within the scope of this paper, have traditionally been used by designers, due to the lack of a better methodology. This is also acknowledged and addressed in this paper.

For such small heat exchangers, Shaukatullah et al. [5] measured the thermal performance for in-line square pin fins and plate heat sinks for different fin thickness, spacing, height, and angle of approach for velocities under 5 m/s, while allowing flow to partially by-pass the exchanger. More recently, Jonsson and Moshfegh [6] experimentally characterized plate and circular,

rectangular and strip pin fins, in both staggered and in-line configurations for different dimensions, allowing for variations on tip and side by-pass. CFD approaches have been extensively applied to study flow and heat transfer in heat sinks, for example by Jonsson and Moshfegh [7], Biber and Belady [8], and Dvinsky et al. [9]. Generally, most of the studies have not been especially useful for extracting local friction or heat transfer coefficients.

Dvinsky et al. [9] used CFD to study in detail flow and heat transfer behavior for in-line and staggered heat sinks for the approach velocities of 1, 3 and 5 m/s. Because their study allowed for both top and side flow by-pass, their results help to elucidate the deficiencies of a simple 2 (or even 4) path model that does not allow for leakage from the heat sink, back to the channel. They found that, when allowing side and top clearance, up to half of the flow that enters the heat sink may leave it through the side and top. CFD simulations of Jonsson and Moshfegh [7] revealed that this leakage flow may be quite complex. They reported inward flow from the sides, to balance flow lost through the top.

This study is motivated by a general lack of data that can be used for heat sink design and optimization of in-line square pin fin heat sinks. The objectives of this paper are to present carefully documented experimental data on the hydraulics and thermal behavior of a consistent set of square pin fin heat sinks of variable height and pitch, and to compare their behavior to that predicted using data for circular tube arrays of infinite (or very long) length available in the literature by a simple ''two-branch by-pass model''.

2. Experimental methods

2.1. Experimental apparatus and measurements

The test geometry is described in Fig. 1a and b. The test apparatus was designed to allow tip by-pass variations but not side by-pass. A duct of rectangular cross-section was constructed with 1.27 cm thick Plexiglas walls and ceiling, and aluminum floor, where the sidewalls and the floor are fixed and the ceiling is movable. The test section is upstream of a flow management section leading to a small centrifugal blower; it operates at sub-ambient pressure, as a way to better control flow and velocity conditions. A quarter-circle cross-section flare was placed at the mouth of the channel, as a smooth contraction from the ambient into the channel. A Pitot tube placed 2.5 cm downstream from the entrance (22.5 cm upstream from the heat sink) measured the total pressure, which was compared to the first static pressure tap, 18 cm from the entrance, to measure approach velocity. Downstream from the channel, a straw pack was used inside a plenum, to reduce unsteadiness and the effects of flow structures on the test section. To adjust the flow velocity within the test section, an AC controller (Variac) was used to control the blower speed. In addition, a flow by-pass gate in the downstream plenum was used for more delicate flow control. During hydraulics testing, the heat sink was placed on the fixed bottom wall, while the top wall was adjusted to allow for tip by-pass at pre-selected typical clearance ratios. This movable wall was equipped with 18 pressure taps distributed on the centerline. The upstream face of the heat sink was located 30 cm from the inlet. A Baratron model 698A differential pressure transducer was utilized to measure static pressure. The pressure transducer with a model 670 signal conditioning unit outputs a voltage that is proportional to the local static pressure. This voltage is a real time signal of the pressure, and is averaged over 3 s (4 s for the SLA model, sampling frequency of 1 kHz), with a National Instruments AT-MIO-16A-2A/D converter. The set-up also includes a scanning valve that allows toggling between the different taps. To account for transient effects, the data was not collected until after the valve was parked for 3 s in the same tap.

During heat transfer testing, the heat sink rests on a 7.5 cm × 5 cm × 2.5 cm Renshape ($k_{rs} = 0.13$ W/m K) base. A 2.5 cm × 2.5 cm, 70 Ω Kapton-encapsulated Nichrome foil heater was used to provide electrical heating. A 0.6 mm thick copper heat spreader was placed between the heater and the heat sink base. The heat sink fits in a seat, such that the floor of the channel is flush with the base of the heat sink, and only the pins protrude. The heat sink was attached to the heater assembly by a thermally conductive adhesive transfer tape. The temperature of the heat sink base was measured using a 36-gauge copper–constantan thermocouple installed in the center of the base through a small well drilled into the side of the base. The thermocouple in the heat sink is connected in series with another thermocouple exposed to ambient air, so that the temperature difference is measured directly. A separate ambient temperature junction was referenced to ice to record the absolute ambient temperature. The thermocouple signals were recorded by a Fluke Hydra 2620 data acquisition unit connected to a personal computer via GPIB. Power was administered to the resistive heater by a 10 W in-house power supply delivering constant power. Typical test power was 10 W, although it was lower for the cases in which the base temperature exceeded 80 °C. Further details can be found in [13].

The thermal performance was measured at approach velocities of $u_{app} = 2$ m/s (±3%) and $u_{app} = 4$ m/s (±1%), while measured dynamic head showed an RMS fluctuation of 7% and 1%, respectively. In the experiments, it was assumed that the steady state conditions were achieved when the change in the base temperature of heat sink was less than 0.5 °C in a time period of 90 s.

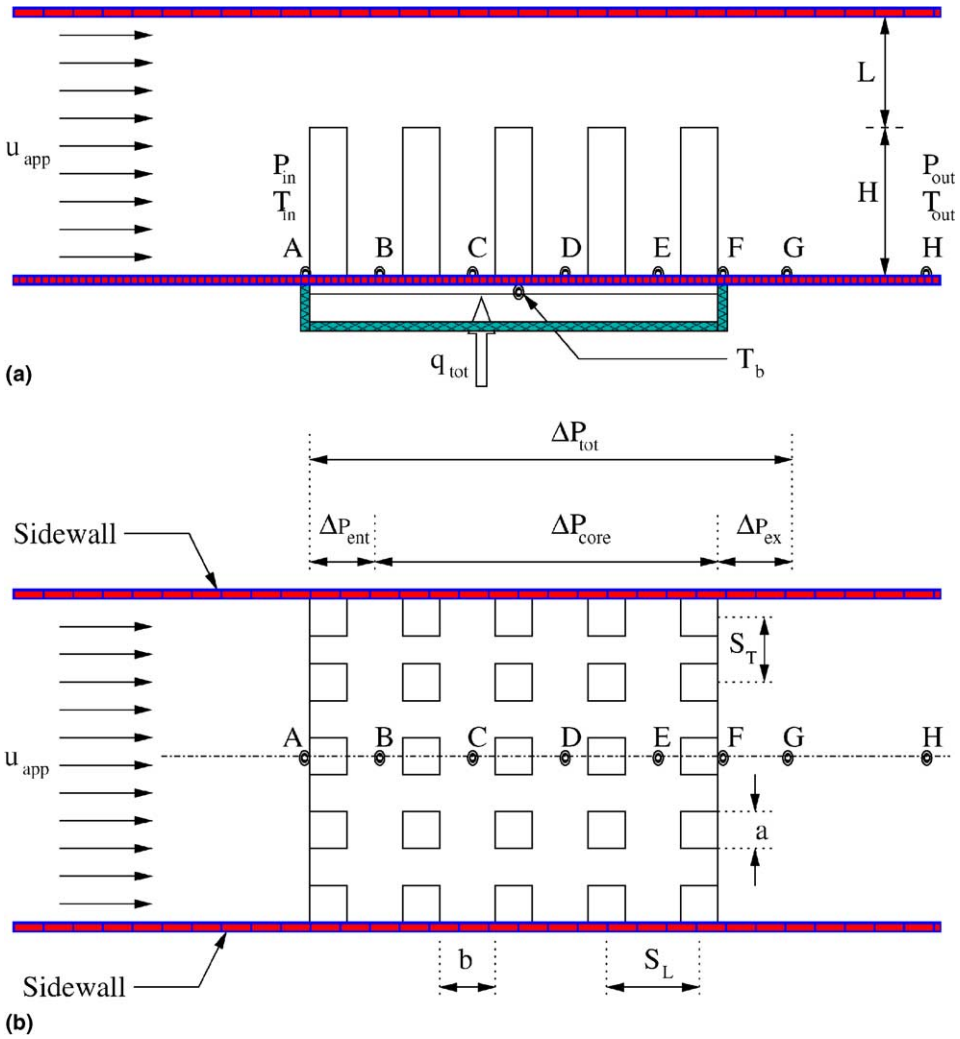

Fig. 1. Illustration of a sample heat sink geometry with a top by-pass channel: (a) side-view and (b) top-view.

When these conditions were achieved, the base temperature, power delivered to the heat sink, and approach velocity were recorded.

The heat sinks used in this study are a subset of the set used by Shaukatullah et al. [5] and are summarized in Table 1. The heat sinks were fabricated from aluminum 2024-T6 ($k_{Al} = 151$ W/m K), using electro-discharge-machining. All of the heat sinks have base dimensions of 25 mm × 25 mm × 2.5 mm where the pin height ranges from 12.5 mm to 22.5 mm. Experiments were conducted on 4×4, 5×5, 6×6, 7×7 and 8×8 pin arrays for $a = 1.5$ mm, and a 5×5 arrangement with $a = 2$ mm and 2.5 mm.

This paper will primarily report on overall pressure drop from the inlet to the exit of the aluminum heat sinks. To evaluate a novel method for measuring pressure distribution within the heat sink, a stereolithography (SLA from here forward) model of heat sink 7C was designed with static pressure taps on the base and on the pins. Location of these internal static taps are shown in Fig. 1a and b. All pin pressure taps have the same orientation.

2.2. Data reduction

The total thermal resistance, R_{th} is the primary thermal performance metric explored in this study. It is defined as

$$R_{th} = \frac{T_b - T_{amb}}{q_{conv}} \tag{1}$$

where q_{conv} is the heat convected through the heat sink surfaces and is given by

Table 1
Geometric description of the heat sinks tested

Desc.	a (mm)	b (mm)	H (mm)	n	$P_L = (a+b)/a$
1A	1.50	1.86	12.50	8	2.238
1B	1.50	1.86	17.50	8	2.238
1C	1.50	1.86	22.50	8	2.238
2A	1.50	2.42	12.50	7	2.611
2B	1.50	2.42	17.50	7	2.611
2C	1.50	2.42	22.50	7	2.611
3A	1.50	3.20	12.50	6	3.133
3B	1.50	3.20	17.50	6	3.133
3C	1.50	3.20	22.50	6	3.133
4A	1.50	4.38	12.50	5	3.917
4B	1.50	4.38	17.50	5	3.917
4C	1.50	4.38	22.50	5	3.917
5A	1.50	6.33	12.50	4	5.222
5B	1.50	6.33	17.50	4	5.222
6A	2.00	3.75	12.50	5	2.875
6B	2.00	3.75	17.50	5	2.875
6C	2.00	3.75	22.50	5	2.875
7A	2.50	3.13	12.50	5	2.253
7B	2.50	3.13	17.50	5	2.253
7C	2.50	3.13	22.50	5	2.253

$$q_{conv} = q_{tot} - q_{loss} \tag{2}$$

T_b is the base temperature of the heat sink measured in the center, T_{amb} is the ambient temperature, q_{tot} is the total amount of power supplied to heat sink, and q_{loss} is the total amount of heat loss due to conduction and radiation.

To estimate the conduction heat losses through the base, a half-symmetry finite element model was constructed utilizing a commercial thermal analysis code. The sides and the bottom of the base module were assumed to be cooled by free convection with a heat transfer coefficient of $3\ W/m^2\ K$. Heat losses from the Renshape bases' upper surface, i.e. the surface which formed part of the channel wall, were modeled using forced convection. Heat transfer coefficients were estimated by temperature measurements of a flat plate in the place of a heat sink, flushed to the floor as well. The flat plate meets the same specifications as the heat sinks, but with no pins, and the measured heat transfer coefficients were approximately $45\ W/m^2\ K$ and $60\ W/m^2\ K$ for approach velocities of 2 m/s and 4 m/s, respectively, nearly independent of the channel height, H. These are the base parameters used in the finite element model. By increasing the free convection coefficient to $4\ W/m^2\ K$ and that of forced to $80\ W/m^2\ K$, an upper bound to the heat losses through these paths was obtained. It was found that the conduction losses were of the order of 10% of the total power. A transient comparison was also made between the cases where pins touched the ceiling, and where a small air gap was present. This comparison showed that tip heat loss by conduction into the ceiling was not influential.

When estimating energy losses due to radiation, the solution was bounded by a plausible worst and best case scenario. To estimate the upper bound, each pin with an emissivity of 0.8 was allowed to transfer heat directly to the surroundings, which was assumed to be a black body at the ambient temperature. For the lower bound, each pin was assumed to be surrounded by a wall at the same temperature and with the same emissivity as that of the pins. Heat was exchanged to the ambient surroundings through the upper plane only, since the bottom plane is the heat sink floor, assumed to be at the pin temperature as well. In this analysis, the view factor of two coaxial finite-height cylinders was used, while keeping the surface areas of the pin and the wall as fixed. Details of the radiation correction model are available in [13].

2.2.1. Uncertainties

Table 2 shows the different sources of uncertainty, a brief description and its value for the pressure measurements. Using this information, for each static pressure measurement, P_{st}, the uncertainty is given by [14]

$$(\delta P_{st})^2 = (\delta P_{A/D})^2 + (\delta P_{DR})^2 + (\delta P_{PT})^2 \tag{3}$$

where the description and the value of the each term is given in Table 2. The uncertainty in the quoted pressure difference across the heat sink is given simply as [14]:

$$(\delta \Delta P_{st})^2 = 2(\delta P_{st})^2 \tag{4}$$

and thus is 40% higher than the uncertainty of the individual static pressure measurement, due to the RMS summation of the individual uncertainties. Typically, the percent uncertainty for a nominal static pressure measurement, $\delta P_{st}/P_{st}$, was on the order of 0.1%, and $\delta \Delta P_{st}/\Delta P_{st}$ was on the order of 0.2%. As in any internal flow testing, the flow unsteadiness induced fluctuations in the instantaneous wall pressure. Time histories show the RMS of the fluctuations to be on the order of 1% of the mean.

Table 2
Sources and description of uncertainty in pressure measurements

Uncertainty	Source	Value (Pa)	Description
$\delta P_{A/D}$	A/D resolution	± 0.03254	12bit, ± 10 V span
δP_{DR}	Signal condition accuracy	$\pm 0.0008P$	0.08% of reading
δP_{PT}	Pressure transducer accuracy	0.0133	100 ppm of 0.1 mmHg

Table 3
Uncertainties in temperature measurements

$T_b - T_{amb}$	$\delta q_{tot}/q_{tot}$	$\delta q_{loss}/q_{loss}$	$\delta R_{th}/R_{th}$
≈0.5 °C	0.5%	20%	≈6–8%

The uncertainty in R_{th}, denoted by δR_{th}, will be a combination of parameters that R_{th} depends on and their individual uncertainty [14]. This relationship is defined in Eq. (5), and the individual uncertainties are summarized in Table 3.

$$\delta R^2 = \left[\frac{\delta(T_b - T_{amb})}{q_{tot} - q_{loss}}\right]^2 + \left[\frac{T_b - T_{amb}}{(q_{tot} - q_{loss})^2}\delta q_{tot}\right]^2 + \left[\frac{T_b - T_{amb}}{(q_{tot} - q_{loss})^2}\delta q_{loss}\right]^2 \quad (5)$$

To determine δq_{loss}, the loss modes were varied as described above. It is relevant to clarify that the uncertainties found by this approach were not necessarily small, but since q_{loss} is small compared to q_{tot}, the impact of individual uncertainties on δR_{th} is small. The uncertainty in R_{th} is typically between 6% and 8%.

3. Experimental results

3.1. Hydraulics

Pressure data were collected for all heat sinks for $CL = 0.00$, 0.25, 0.50, 1, 2, and 3 with approach velocities of, $u_{app} = 2$ m/s and 4 m/s. Additional tests were performed for $CL = 4$ with the heat sinks of $H = 12.5$ mm and 17.5 mm at the same approach velocities. For all cases, the total pressure drop, ΔP_{tot}, was determined by using the lowest pressure upstream of the heat sink, and the highest pressure downstream from the heat sink.

Figs. 2 and 3 show the pressure profiles of the channel for heat sinks 1C and 4C for $u_{app} = 4$ m/s. These two cases correspond to the tallest, densest, and most sparse heat sinks, for $a = 1.5$ mm. As expected, the pressure drop decreases as CL and b increase, with diminishing effects from pin spacing at higher clearances. This behavior is consistent with the set, and can also be appreciated in Fig. 4. It should be noted that the pressure increases on the pressure tap directly in front of the heat sink. This profile is thought to be due to stagnation as the flow encounters the obstruction. The taps (on the span-wise center line) lie in front of or behind a pin and this will be the case for all heat sinks with an odd number of pins per row, but in between pins for heat sinks with an even number of pins per row. Thus, interpretation of these local effects should be done with care.

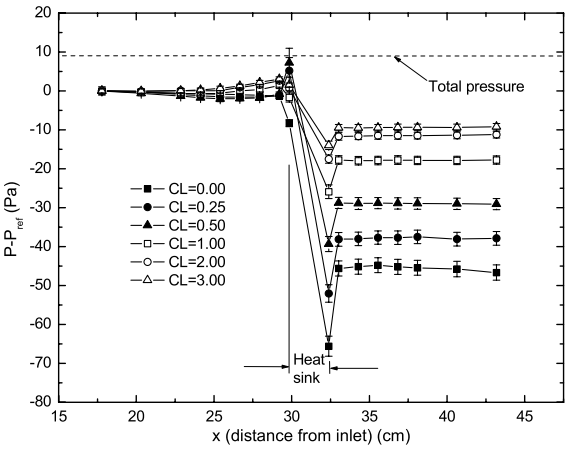

Fig. 2. Channel pressure distribution for 1C, at $u_{app} = 4$ m/s and various clearance ratios.

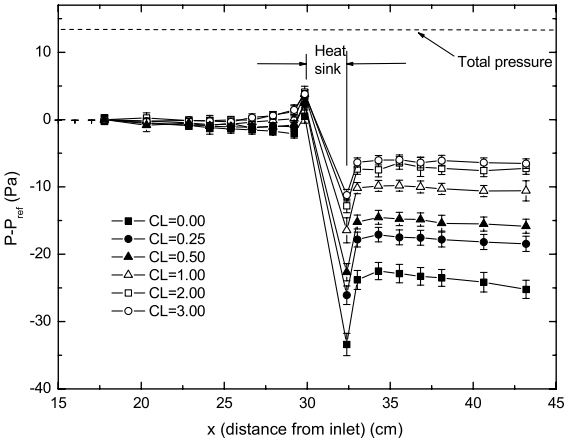

Fig. 3. Channel pressure distribution for 4C, at $u_{app} = 4$ m/s and various clearance ratios.

The acceleration at the inlet of the heat sink leads to an inlet pressure drop, however this could not be observed in the data, as there were no pressure taps in the heat sink interior. The pressure increase and recovery are more dramatic in 1C compared to those of 4C, possibly due to the local position of the tap in question.

Fig. 4 shows the effects of pitch size on total pressure drop vs. clearance ratio (CL) for all of the heat sinks of $H = 22.5$ mm tested with $u_{app} = 4$ m/s. It can be seen that the effect of heat sink geometry diminishes as the by-pass increases. At $CL = 0$, ΔP_{tot} span is 22 Pa, while at $CL = 3.0$, it is only 5 Pa. The upper bound shown in Fig. 4 is for a solid aluminum block of height $H = 22.5$ mm which represents a heat sink with $P_L = 1$. It can be noted that the non-dimensional transverse pitch alone does not seem to fully capture

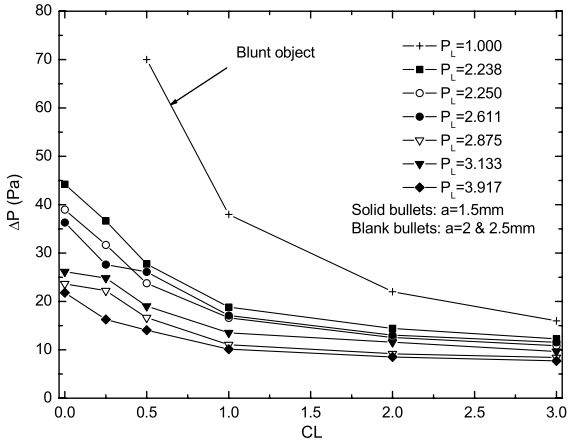

Fig. 4. Total pressure drop vs. clearance ratio for $H = 22.5$ mm at $u_{app} = 4$ m/s and various P_L's.

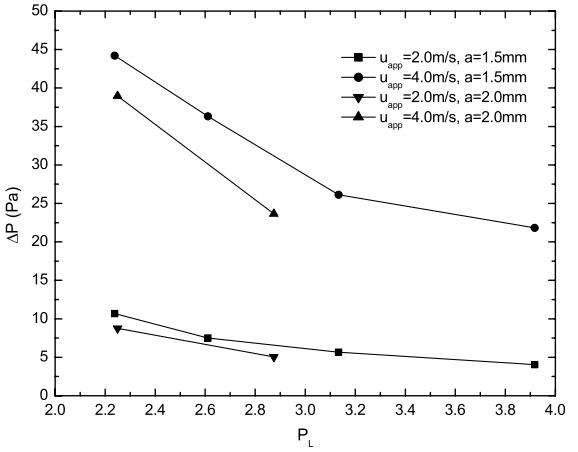

Fig. 5. Pressure drop vs. non-dimensional pitch for $a = 1.5$, 2, 2.5 mm and $H = 22.5$ mm at zero clearance.

the geometrical effects on the flow behavior in such short pin fin heat sinks. For a constant pin diameter, pressure drop monotonically increases with decreasing pitch. However, changing the pin diameter alters this behavior considerably. This may be due to a change in the number of rows. For instance, heat sink 7C, which has five rows, has almost the same non-dimensional pitch as 1C, which has eight rows. Likewise, 6C (five rows) behaves more closely to 4C (five rows) than 3C (six rows) and 2C (seven rows).

The experimental data demonstrated inconsistent behavior for $CL = 0.25$ and 0.50 for both $u_{app} = 2$ m/s and 4 m/s. The trend of increasing ΔP_{tot} with decreasing CL was reversed, or ΔP_{tot} was measured to be higher than for the $CL = 0$ case, for a given heat sink. At low clearances, pressure measurements did not exhibit high repeatability. Discrepancies up to 10% were found between identical tests. Data for $CL = 0.25$ and 0.50 reveal interesting trends, but should be viewed as tentative.

Fig. 5 shows ΔP_{tot} vs. P_L data for $u_{app} = 2$ and 4 m/s, and $CL = 0$. It clearly illustrates the pressure drop dependence on the fin spacing and the fin diameter. This curve will reach infinity in the case of $P_L = 1$, and its minimum value in the case of $P_L \to \infty$. For a given d_f and u_{app}, overall pressure drop increases with a decreasing non-dimensional longitudinal pitch, as expected. However, keeping the non-dimensional pitch size fixed as the number of fins and fin diameters are changed at a given approach velocity, there is a significant difference between two data sets corresponding to two different fin diameters. Hence, as mentioned previously, there is clearly a separate dependence on pin diameter.

Fig. 6 shows static pressure measurements conducted within the core of the SLA heat sink 7C as illustrated in Fig. 1a. The positions of the static taps follow the labelling shown in Fig. 1a and b. The heat sink was fabricated using the SLA rapid prototyping technique, which made it possible to build numerous static pressure ports rather easily. Discrepancy was observed in ΔP_{tot} measure for the SLA prototype, and the aluminum version of the same heat sink (7C). This is believed to be a result of differences in the dimensions due to shrinkage of SLA model, as well as differences in surface finish. Nevertheless, these local core pressure measurements clearly show the inlet pressure drop, and the exit pressure recovery.

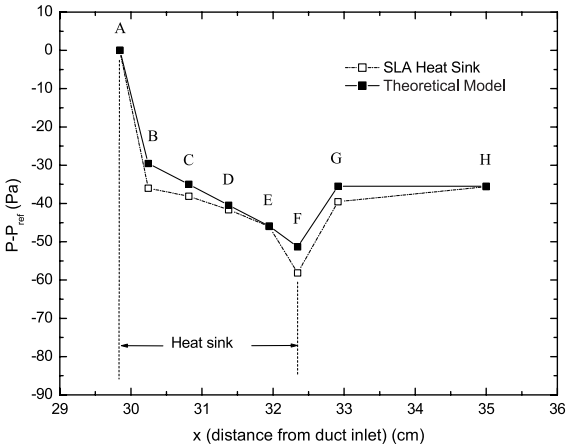

Fig. 6. Comparison of the experimental pressure distribution inside the heat sink (SLA model) with the theoretical pressure distribution for heat sink 7C at $CL = 0$ and $u_{app} = 4$ m/s.

3.2. Heat transfer

Thermal resistance was measured for the heat sinks described in Table 1 for the approach velocities of 2 and 4 m/s. Heat sink geometry C3 was evaluated at dif-

ferent velocities to examine its flow velocity dependence on thermal resistance and the results are shown in Fig. 7. Above 2.4 m/s, a dependence on approach velocity of a power of 0.73 was found, while below 2.4 m/s, a trend on u_{app} to the power of 0.42 was observed. It should be noted that the thermal resistance uncertainty for lower velocities tends to be higher and conduction heat losses become comparable to the heat convected. This may skew the data below 2.0 m/s. The clear shift in the flow regime is almost certainly due to transition to turbulent flow, however no direct measure of transitional flow was made, therefore, this is speculative.

Fig. 8 shows the thermal resistance against non-dimensional pitch and height at $u_{app} = 4$ m/s. Thermal resistance increases with diminishing height, and the effect is more pronounced for shorter pins. In fact, Metzger et al. [15] reported a *Nu* correlation up to 30–35% lower compared to that of infinitely long tubes in the case of very short ($H/d_f = 1$) pins. For shorter pins, the floor becomes an important heat transfer area, with a lower local heat transfer coefficient compared to the pins. As the pins grow taller, the exposed area in surfaces with higher local heat transfer rates increases, with a compounding effect. As the pitch decreases, the thermal resistance decreases due to increased surface area, as the pin count increases, and higher Nusselt numbers [12] are obtained, as the average fin velocity increases.

Another way to look at the same data is to define a heat transfer coefficient, h based on log-mean temperature difference, ΔT_{lm}, fin efficiency of unity, and the wetted heat sink area, A_w,

$$h = \frac{q_{conv}}{A_w \Delta T_{lm}} \tag{6}$$

Since h is defined on the total area, and since the local heat transfer coefficients on the floor are lower than those on the pin [15], variations of pin height cause variations in h due to changes in the flow. Also, variations in h are due to increased importance of the unpinned base area, A_b. It was seen that this effect is not so pronounced between $H = 22.5$ mm and 17.5 mm (a 22% decrease in height corresponding to a decrease of 11% in h) as it is between 17.5 mm and 12.5 mm (a 29% decrease in height corresponding to a decrease of 31% in h). As pitch increases, the floor area to pin area increases (for any given height) and thus h loses value as a pin heat transfer coefficient, making a poor comparison between varying P_L for the same H.

Fig. 9 presents *Nu*, based on h defined by Eq. (6), vs. Re_{av} for a pin height of $H = 22.5$ mm. Re_{av} is based on the local velocity averaged over the surfaces of the tubes

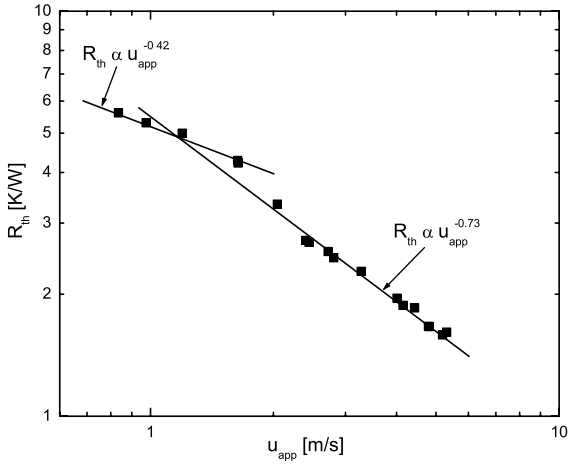

Fig. 7. Thermal resistance vs. approach velocity for heat sink 3C at zero clearance.

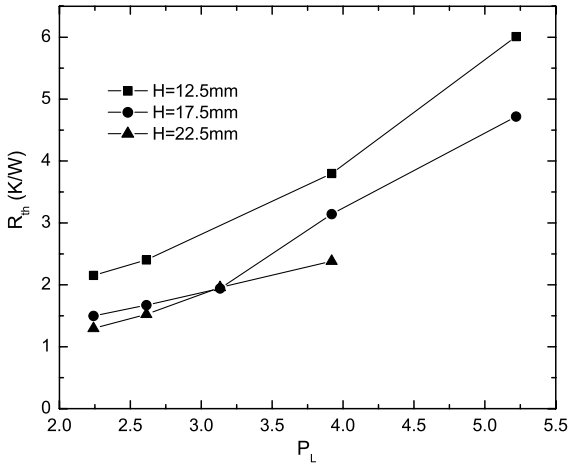

Fig. 8. Thermal resistance vs. non-dimensional pitch for $a = 1.5$ mm at $u_{app} = 4$ m/s and zero clearance.

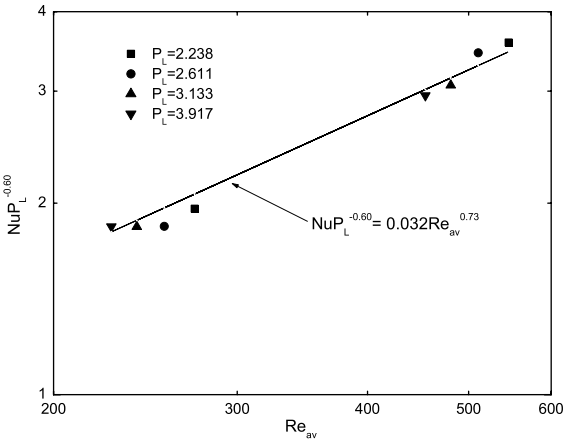

Fig. 9. *Nu* vs. Re_{av} for $H = 22.5$ mm and $a = 1.5$ mm at $u_{app} = 2$, 4 m/s and zero clearance.

or fins [12]. This data set is correlated to within 6% by the expression:

$$Nu = 0.032 Re_{av}^{0.73} P_L^{0.60} \quad (7)$$

Although Nu carries the same limitations as h regarding the loss of validity as P_L increases and the limited span of Re_{av}, this correlation serves as a reference for comparison to classical correlations for tube bundles.

The influence of top clearance ratio on the thermal resistance is shown in Fig. 10. R_{th} has a relatively low sensitivity to CL for a given P_L since the heat transfer coefficients are dependent on $Re_{av}^{0.73}$ rather than linearly. Experimental results from the hydraulics part shows that a heat sink with by-pass flow will have lower flow rates through the pin array, and if the equivalent flow rate is imposed, the same heat sink without by-pass will have the same pressure drop. As by-pass is allowed, the flow through the array diminishes, leading to decrease in the convective heat transfer coefficient and increase in the thermal resistance.

Fig. 11 presents the variation of R_{th} vs. P_L at various clearance ratios. Sparser heat sinks exhibit greater clearance ratio dependence than denser heat sinks even though the by-pass ratio is higher in the latter. If $CL \neq 0$, as the pitch continues to decrease, a minimum is expected, where the increasing wetted area is not enough to balance the decreasing heat transfer rates due to diminishing flow through the array. Jubran et al. [16] found the optimum to occur at $P_L = 2.5$, for circular pins interacting with floor and $H/d_f = 9.4$. Although this optimal pitch was not achieved with the heat sinks tested, it was examined with the model developed. Further discussion will be given as a case study in a concluding section of this paper.

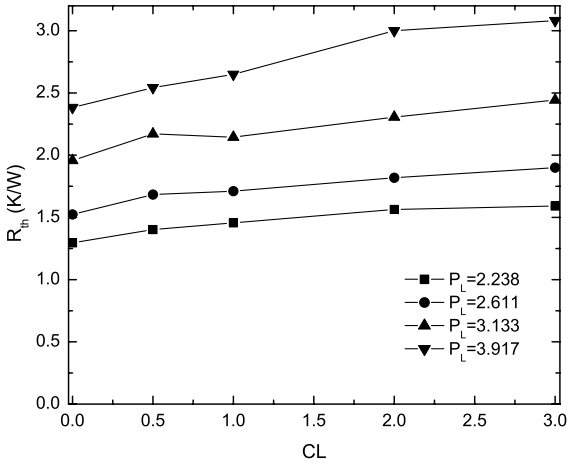

Fig. 10. Thermal resistance vs. clearance for $H = 22.5$ mm and $a = 1.5$ mm at $u_{app} = 4$ m/s.

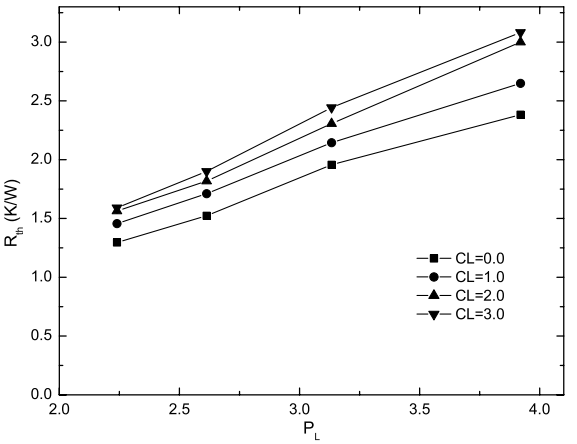

Fig. 11. Thermal resistance vs. non-dimensional pitch for $H = 22.5$ mm and $a = 1.5$ mm at $u_{app} = 4$ m/s and various clearance ratios.

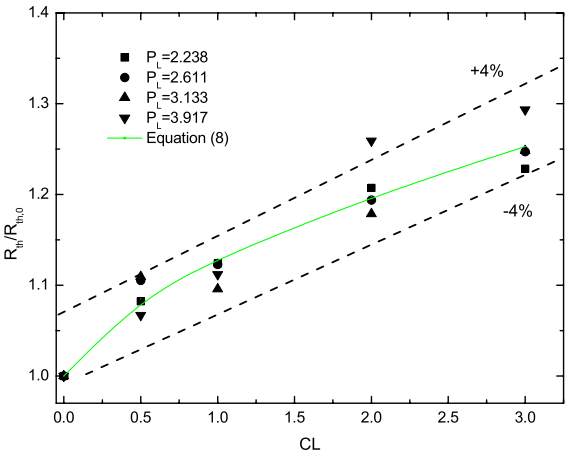

Fig. 12. Thermal resistance (R_{th}) normalized with zero clearance thermal resistance ($R_{th,0}$) vs. clearance ratio for $H = 22.5$ mm and $a = 1.5$ mm at $u_{app} = 4$ m/s.

In Fig. 12, the thermal resistance at different clearance ratios has been normalized by the corresponding zero clearance thermal resistance, $R_{th,0}$. It can be seen that the increase of relative thermal resistance due to clearance ratio lies within a $\pm 4\%$ band (well within uncertainty limits, estimated to be ≈6–8%) about the linear fit. The increase in thermal resistance from $CL = 0$ to $CL \to \infty$ approaches 25% for all heat sinks. For this particular pitch and fin height, the normalized thermal resistance is fit well by the correlation:

$$R_{th}/R_{th,0} = 1 + aCL^n \quad (8)$$

where the constant a and the power exponent, n are determined to be 0.13 and 0.608, respectively.

4. Computational analysis

Given the mass flow rate and the total pressure of the air at the inlet of the heat sink in addition to the geometric parameters, pressure drop can be determined on a differential basis by utilizing a simple one-dimensional model, which incorporates empirical friction factor relations. Most generally, a duct can be composed of two different sections, namely a finned section (heat sink) and a by-pass channel at the top of it as shown in Fig. 1a. The "two-branch by-pass model" assumes that mass flow rate entering either section does not change along the flow direction, in other words, tip leakage from the finned section to the by-pass channel is neglected and therefore, mass flow rate remains constant in each section. For the sake of space, only important details are given here. Interested readers should refer to [17,18] for the complete formulation.

Since the drag for complex flows cannot be expressed analytically, it is customary to introduce an empirical drag or friction factor defined in a form suggested for example by Zhukauskas [12] for circular tube bundles. The total pressure drop experienced in a heat sink should also include the entrance and the exit effects of the heat sink. This situation is illustrated in Fig. 1b and the total pressure drop for the heat sink can be written as

$$\Delta P_{\text{tot}} = \Delta P_{\text{ent}} + \Delta P_{\text{core}} - \Delta P_{\text{ex}} \tag{9}$$

where ΔP_{ent} is the pressure drop at the entrance of the heat sink, ΔP_{core} is the pressure drop due to the fins, and ΔP_{ex} is the pressure rise at the heat sink exit. Referring to Fig. 1b, they can also be expressed in the form such as

$$\Delta P_{\text{ent}} = P_{\text{in}} - P_B \tag{10}$$

$$\Delta P_{\text{core}} = P_B - P_F \tag{11}$$

$$\Delta P_{\text{ex}} = P_G - P_F \tag{12}$$

The terms, ΔP_{ent} and ΔP_{ex} are shown separately in Eq. (9), since they comprise both frictional and inviscid effects due to the geometry change, i.e. contraction and expansion at the entrance and expansion at the exit. For the comparisons made in this paper, ΔP_{ent}, ΔP_{ex} are determined based on the loss coefficients from Fig. 5.3 of [10] for a simple, two-dimensional rectangular contraction or expansion. It should be noted that the entrance pressure drop includes a contraction into the first pin row followed by an expansion out of the pin row.

In order to design and optimize fin heat sinks, it is necessary to predict the heat transfer by the combined conduction through the pins and convection from their surfaces. Experimentally, it is difficult to measure pin by pin heat transfer coefficients and far easier to measure overall base to ambient thermal resistance. The one-dimensional model requires the specification of a local pin-averaged heat transfer coefficient; hence, the model can be used to test the validity of correlations for the specified heat transfer coefficient by comparing measured and predicted overall thermal resistances. This approach is illustrated in the following section. Specification of the heat transfer coefficients on the base area is ad hoc due to the absence of local data.

The hydraulics problem is first solved to determine the average velocity in the finned section. Since the tip leakage is neglected, the energy balance per fin row in the finned section is written as

$$q_{\text{f,r}} + \dot{m} c_p T_x = \dot{m} c_p T_{x+\Delta x} \tag{13}$$

where $\dot{m}$ is the mass flow rate in the finned section, c_p is the specific heat of the fluid, and $q_{\text{f,r}}$ is the rate of heat transfer per unit time per row. If the outlet mixed mean fluid temperature is written in terms of its Taylor series with second and higher order terms neglected, the increase in mixed mean temperature of the fluid per row can be determined from

$$\Delta T = \frac{q_{\text{f,r}}}{\dot{m} c_p} \tag{14}$$

and the total heat transfer rate convected through the heat sink can be written as

$$q_{\text{conv}} = \sum_{i=1}^{n_{\text{r}}} (q_{\text{f,r}})_i \tag{15}$$

where n_{r} is the number of fin rows.

If the base temperature of the heat sink, T_{b} is averaged and assumed to be constant, the total convective heat transfer rate from the heat sink to the fluid per row can be written as

$$q_{\text{f,r}} = \eta_{\text{o}} h (n_{\text{f}} A_{\text{f}} + A_{\text{b}})(T_{\text{b}} - T) \tag{16}$$

where η_{o} is the overall surface efficiency, n_{f} is the number of fins per row, A_{f} is the exposed surface area of a single fin, A_{b} is the corresponding base surface area for a given control volume, and T is the local mixed mean air temperature. Note that the heat transfer coefficient of the base area is taken to be the same as for the fins. For closely spaced infinitely long circular tube bundles, the empirical Nu correlation proposed by Zhukauskas for circular tubes [12] at low velocities appears to be a good first order approximation for square pin fins and has been used to determine the heat transfer coefficients in this study.

4.1. Methodology

Pressure drop for the heat sinks with no by-pass can simply be determined by using the developed one-dimensional model marched in the flow direction. With by-pass, prediction of the pressure drop in the heat sink

requires an iterative procedure as shown in [17,18] because both the flow partitioning and the overall pressure drop are unknown. If there is a by-pass channel, the model first assumes that the inlet velocity of the air for the two sections is the same, then by decreasing the velocity of the air in the finned section and therefore, by increasing the velocity of the air in the by-pass duct according to the conservation of mass requirements, a convergent solution is sought where the exit static pressure (at station G of Fig. 1 is the same in the by-pass and finned branches. The model calculates the exit static pressures for both of the sections and determines whether they are equal. They are assumed to be equal if the difference in pressures is less than 0.5% (specified convergence criteria) with respect to the pressure drop of the finned section. This procedure is repeated until the equal exit static pressures are obtained.

5. Results and discussion

5.1. Hydraulics

Fig. 6 demonstrates the comparison between the measured static pressure in the SLA prototype of heat sink 7C and the predicted pressure using the one-dimensional hydraulic model, utilizing the core friction coefficients from Zhukauskas [12] for arrays of infinitely long circular tubes, and the inlet and exit loss coefficients from Kays and London [10]. For this single test case, the computational model predicts the pressure behavior well. There is a good agreement for all of the separate sections, i.e. the inlet and the core pressure drop and the exit recovery. It is also noteworthy that the inlet pressure drop is as significant as the core pressure drop in the overall flow resistance for the heat sinks tested. The difference between the core pressure drops is most likely due to the end-wall and entrance region effects; correlations in [12] were developed for banks of long tubes with many tube rows, in which most of the flow was in the fully developed region. That might not be the case for the short heat sink used in the experiments. Furthermore differences are expected between tubes with square and round cross-section.

Fig. 13 demonstrates the overall pressure drop at various clearance ratios for two different non-dimensional pitches of 2.238 and 3.917, which correspond to the densest and the most sparse in-line fin arrangements, respectively, at a fin height of $H = 22.5$ mm. At high clearance ratios, there is a good agreement between the theoretical predictions and the experimental results despite the poor agreement of the loss coefficients as shown in [17]. However, the discrepancy between the results increases as the clearance ratio decreases. This discrepancy once again may be attributed to the discrepancies in the core.

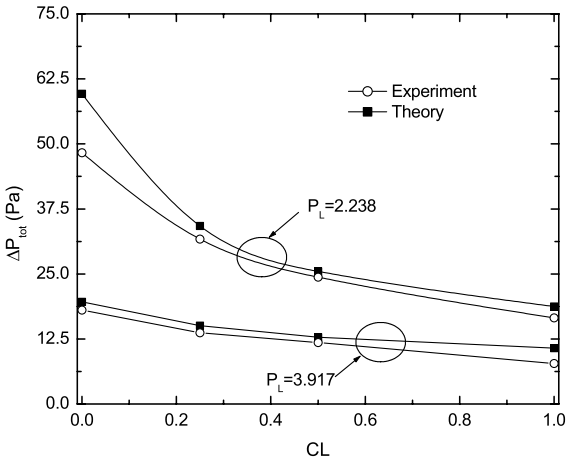

Fig. 13. Comparison of the measured and the predicted total pressure drop as a function of clearance ratio for $P_L = 2.238$ and 3.917 at $u_{app} = 4$ m/s (tallest heat sinks), $H = 22.5$ mm.

5.2. Heat transfer

Although it is not possible to compare local behavior, comparison of the predicted overall thermal resistance with the data is a useful exercise in determining the accuracy of the one-dimensional model and the ad hoc circular tube correlations used for the heat transfer coefficients. Fig. 14 presents the experimental thermal resistance results and corresponding computational predictions of the heat sink with $P_L = 3.133$ in the approach velocity range of $0.8 \leqslant u_{app} \leqslant 5.3$ m/s. At low approach velocities, the discrepancy between the theoretical and the experimental results is about 34%. At higher approach velocities, $u_{app} \geqslant 3.0$ m/s, there is good

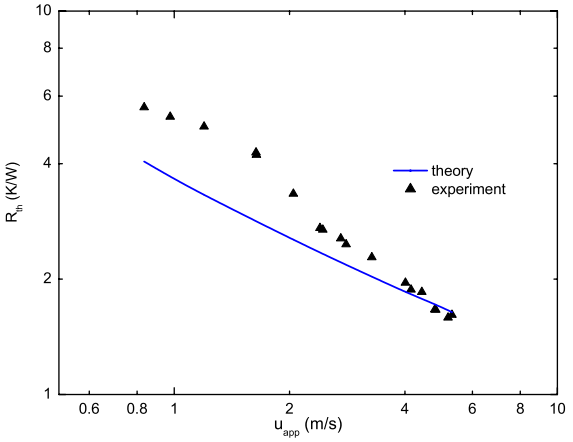

Fig. 14. Comparison of the experimentally determined and the predicted thermal resistance vs. approach velocity for $P_L = 3.133$ and $H = 22.5$ mm at zero clearance.

agreement. A similar behavior was observed in the case of hydraulic resistance. For this particular case, the power dependence of Nu on Re_{av}, thus that of h on u_{app} is about 0.5 for the recommended empirical correlations of circular tube bundles [12]. For the present experiments, this power-law exponent is 0.42 for the approach velocities less than 2.4 m/s and 0.73 for the higher velocities. This discrepancy suggests a possible failure of the correlation shown in [12] in both the laminar and turbulent regimes owing to differences between circular and square tube behavior, and end-wall effects.

In order to explore the effect of heat sink height, H, experiments and computations were performed for three different cases of $H = 12.5$, 17.5 and 22.5 mm at $u_{app} = 2$, 4 m/s. The results are shown as R_{th} vs. P_L for the tallest and shortest heat sinks only in Fig. 15. Taller pins not only have a larger surface area, but also have a higher heat transfer coefficient as a result of diminishing end-wall effects and pin-base interaction. At higher approach velocities, computational results match well with those of experiments, surprisingly, even for the shortest heat sinks. Decreasing the heat sink height, the discrepancy between the experimental results and theoretical predictions increases, with the worst occurring for the shortest heat sink with $u_{app} = 2$ m/s, at the largest pin spacing. It is hypothesized that end-wall effects are greatest for the shortest heat sinks; hence departure from the correlation shown in [12] is the greatest in that case, at low velocities. These plots also demonstrate a monotonic trend of increasing thermal resistance with increasing pitch, which can be attributed to a decrease of surface area at higher non-dimensional pitch sizes for an equal size base area. As the pitch, or pin spacing increases, the exposed base area, A_b, becomes a larger percentage of the total area. Hence, the assumption that the heat transfer is the same on the pins and on the base may become poorer at larger pin spacing.

The one-dimensional model can also be compared to data in the cases with tip clearance. It should be remembered that tip leakage is not taken into account for this model and may inherently introduce error. Fig. 16 demonstrates the thermal resistance against the clearance ratio at $P_L = 2.238$ (the densest configuration) and $P_L = 3.917$ (the sparsest configuration). For the densest configuration, there is excellent agreement between the theory and the experiments in the case of $u_{app} = 4$ m/s especially at high clearance ratios. The agreement is even better for $P_L = 3.917$. However, the discrepancy between the results increases if u_{app} is decreased to 2 m/s, where the worst case is obtained at zero clearance and the error between the results is up to 32% at $P_L = 2.238$. While not shown here, a similar behavior can also be seen for non-dimensional pitch sizes of $P_L = 2.611$ and 3.133. Regardless of the pitch and the approach velocity, both of the theoretical predictions

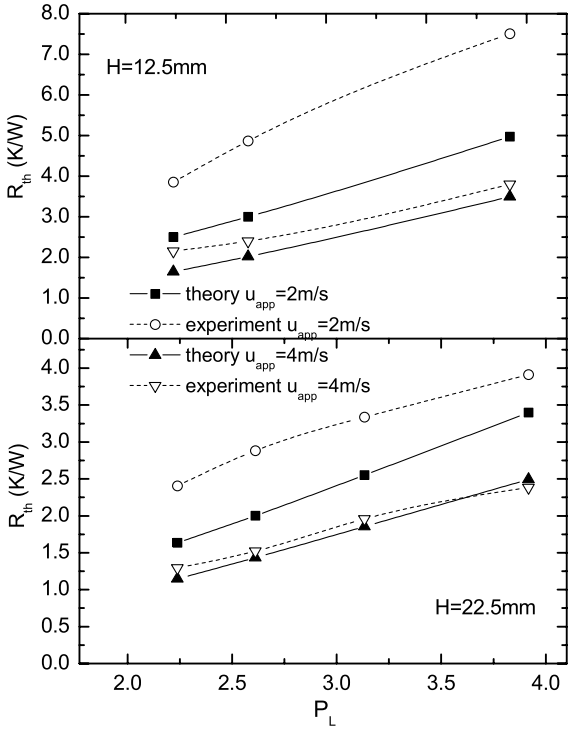

Fig. 15. Comparison of the experimentally determined and the predicted thermal resistance vs. non-dimensional pitch for $H = 12.5$ and 22.5 mm at $u_{app} = 2$, 4 m/s and zero clearance.

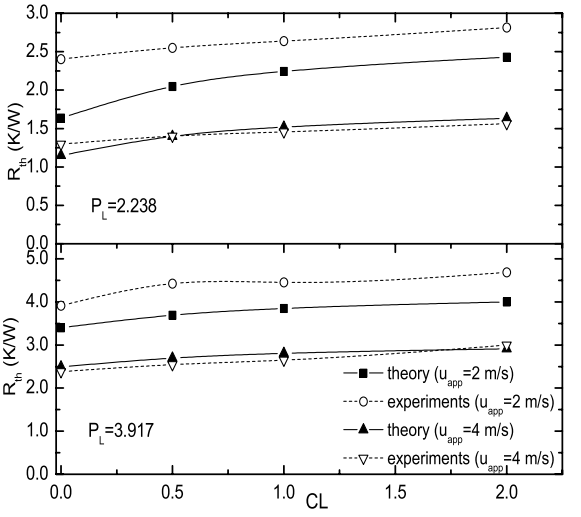

Fig. 16. Comparison of the experimentally determined and the predicted thermal resistance vs. clearance ratio for $H = 22.5$ mm and $P_L = 2.238$ and 3.917 at $u_{app} = 2$, 4 m/s.

and the experimental data follow the same trend with the increasing clearance ratio.

5.3. Case study: heat sink optimization

In designing electronic packages, major constraints are the highest temperature and the geometric features of the package. Due to a limited space in many applications, optimization of the heat sinks is one of the major issues to be taken into consideration in electronic equipment design. Although one of the main goals of this paper is to investigate the applicability of infinitely long tube correlations to compact heat exchangers rather than conducting a detailed heat sink optimization, a case study was performed for the optimization of heat sinks utilized in the experimental study, since this is the final step in electronics cooling if the design constraints mentioned above are specified.

In this case study, it is intended to determine the optimum number of fins for a fixed size of heat sink base (25 mm × 25 mm), height ($H = 22.5$ mm) and a fin diameter ($d_f = 1.5$ mm). In addition, the base temperature, T_b is assumed to be constant and the approach velocity is taken to be $u_{app} = 4$ m/s. For the given conditions, a simple optimization can be performed by analyzing the variation of thermal resistance with respect to pitch size, or number of fins. Fig. 17 illustrates this case at various clearance ratios. For the clearance ratios of 0.5, 1.0 and 2.0, the minimum thermal resistance is obtained at $P_L = 1.96$, where the corresponding number of fins is 9. This is lower than that of predicted by Jubran et al. [16], who determined an optimum of $P_L = 2.5$. It was already shown that flow by-pass increases with decreasing pitch, therefore further reduction of the pitch does not decrease the thermal resistance as the fin velocity decreases with increasing by-pass ratio.

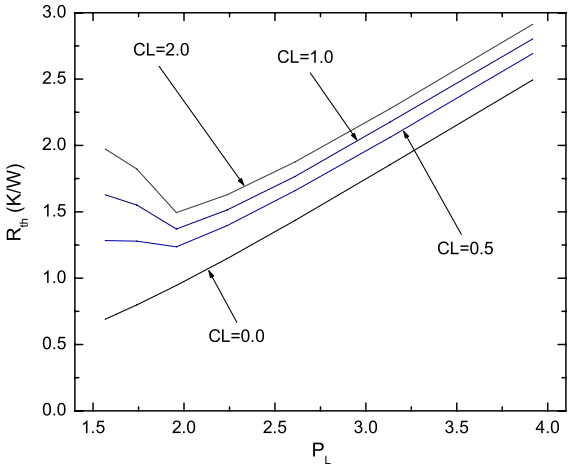

Fig. 17. Thermal resistance vs. non-dimensional pitch at various clearance ratios for $H = 22.5$ mm at $u_{app} = 4$ m/s.

6. Conclusions

Pressure drop, and by-pass ratio results were presented for in-line pin square pin fin heat sinks with various pitch sizes. A two-branch by-pass model was developed and the results extracted from the model were compared with those of experiments. In order to make detailed pressure measurements, a SLA model was built and tested.

Thermal resistance and performance results were shown for in-line pin square pin fin heat sinks with various pitch sizes. A computational model was derived and the model predictions were compared with the experimental data. A case study was performed to demonstrate the fin optimization problem for certain design constraints.

Based on the results of the present study, the following conclusions can be drawn:

- In determining the hydraulic resistance of heat sinks, infinitely long tube bundle correlations can be used with a reasonable accuracy, however end-wall, entrance and exit effects may result in a considerable difference between theoretical predictions and experimental results.
- The commonly used pressure loss and heat transfer coefficients for tube bundles, for example in [12], represent fully turbulent and fully developed conditions. Neither of these are representative of conditions in air-cooled heat sinks, therefore new experimental data at low Re and in developing regions is very much needed.
- Comparison of SLA measurements with theoretical predictions shows that the estimation of entrance and exit effects is important; poor estimation of these may lead to significant differences in determining the overall pressure drop.
- Overall thermal resistances for fixed pin height and zero by-pass suggest laminar behavior below approach velocities of 2.4 m/s, and turbulent behavior above 4 m/s.
- For fixed pin diameter and height, the area averaged Nusselt number scales approximately as $P_L^{-0.6}$ and $Re_{av}^{0.73}$.
- Variations in overall thermal resistances due to variation of pin height and pitch are not well correlated solely to variations in total area, suggesting that there are important differences between the heat transfer coefficients on the pins and on the base area.

- For the tallest pins, the overall thermal resistance increases by no more than 25% from its zero clearance value to its value at a clearance ratio of 3.0. The thermal resistance scales as CL^n, where n equals 0.608 (Fig. 12).
- The conventional heat transfer correlations for circular tube bundles were only moderately successful for predicting pin fin heat sink thermal performance. The model significantly underestimated the thermal resistance at low velocities and was in good agreement at higher velocities.
- The two-leg by-pass model adequately predicted the effects of flow by-pass on the overall thermal resistance, in the turbulent flow regime, suggesting that the heat transfer from the heat sink surfaces is set almost completely by the local fin velocity. Apparently, tip leakage effects are minor.
- The optimal pin spacing that minimizes the overall thermal resistance, at fixed approach velocity, is predicted to be $P_L \approx 2.0$ by the model. This was not experimentally verified.

Acknowledgement

This work was made possible by grants from the Intel Corporation, Platform Architecture Laboratory, and Cisco Systems through the University Research Program.

References

[1] R.W. Knight, J.S. Goodling, D.J. Hall, Optimal thermal design of forced convection heat sinks-analytical, ASME J. Electron. Packaging 113 (1991) 313–321.
[2] P. Teertstra, M.M. Yovanovich, J.R. Culham, T. Lemczyk, Analytical forced convection modeling of plate fin heat sinks, in: Proceedings of the Fifteenth IEEE SEMI-THERM Symposium, San Diego, CA, 1999, pp. 34–41.
[3] S. Lee, Optimum design and selection of heat sinks, in: Proceedings of the Eleventh IEEE SEMI-THERM Symposium, San Jose, CA, 1995, pp. 48–54.
[4] M.A. Butterbaugh, S.S. Kang, Effects of airflow by-pass on the performance of heat sinks in electronics cooling, ASME Adv. Electron. Packaging 10 (2) (1995) 843–848.
[5] H. Shaukatullah, W.R. Storr, B.J. Hansen, M.A. Gaynes, Design and optimization of pin fin heat sinks for low velocity applications, in: Proceedings of the Twelfth IEEE SEMI-THERM Symposium, Austin, TX, 1996, pp. 151–163.
[6] H. Jonsson, B. Moshfegh, Modeling of the thermal and hydraulic performance of plate fin, strip fin, and pin fin heat sinks–influence of flow by-pass, IEEE Trans. Components Packaging Technol. 24 (2) (2001) 142–149.
[7] H. Jonsson, B. Moshfegh, Enhancement of the cooling performance of circular pin fin heat sinks under flow by–pass conditions, in: Proceedings of the Eighth IEEE Inter Society Conference on Thermal Phonomena (ITHERM), San Diego, CA, 2002, pp. 425–432.
[8] C.R. Biber, C.L. Belady, Pressure drop predictions for heat sinks: what is the best method? ASME Adv. Electron. Packaging 19 (2) (1997) 1829–1835.
[9] A. Dvinsky, A. Bar-Cohen, M. Strelets, Thermofluid analysis of staggered and inline pin fin heat sinks, in: Proceedings of the Seventh IEEE Inter Society Conference on Thermal Phonomena (ITHERM), Las Vegas, NV, 2000, pp. 157–164.
[10] W.M. Kays, A.L. London, Compact Heat Exchangers, Krieger, Malabar, Florida, 1998 (Chapter 5).
[11] I.E. Idelchik, Flow Resistance: A Design Guide for Engineers, Hemisphere, New York, 1989.
[12] A. Zhukauskas, Heat transfer from tubes in cross flow, in: J.P. Hartnett, T.F. IrvineJr. (Eds.), Advances in Heat Transfer, 8, Academic Press, San Diego, 1972, pp. 93–160.
[13] M. Urdaneta, Characterization of pressure drop and heat transfer on pin fin heat sinks under side-inlet side-exit configuration with top and side flow by-pass, M.S. Thesis, The University of Arizona, Tucson, Arizona, 2002.
[14] R.J. Moffat, Describing the uncertainties in experimental results, Exp. Therm. Fluid Sci. 1 (1) (1988) 3–17.
[15] D.E. Metzger, Z.X. Fan, W.B. Shepard, Pressure loss and heat transfer through multiple rows of short pin fins, in: Proceedings of the Seventh International Heat Transfer Conference, Hemisphere, Washington, DC, vol. 3, 1982, pp. 137–142.
[16] B.A. Jubran, M.A. Hamdan, R.M. Abdualh, Enhanced heat transfer, missing pin and optimization for cylindrical pin fin arrays, ASME J. Heat Transfer 115 (3) (1993) 576–583.
[17] M.B. Dogruoz, M. Urdaneta, A. Ortega, R.V. Westphal, Experiments and modeling of the hydraulic resistance of in-line square pin fin heat sinks with top by-pass flow, in: Proceedings of the Eighth IEEE Inter Society Conference on Thermal Phenomena (ITHERM), San Diego, CA, 2002, pp. 251–260.
[18] M.B. Dogruoz, M. Urdaneta, A. Ortega, Experiments and modeling of heat transfer of in-line square pin fin heat sinks with top by-pass flow, ASME Heat Transfer Div. Publ.-HTD 372 (7) (2002) 195–206.